applied optics

Optimization of optical properties of photonic crystal fibers infiltrated with carbon tetrachloride for supercontinuum generation with subnanojoule femtosecond pulses

Quang Ho Dinh,[1] Jacek Pniewski,[2,*] Hieu Le Van,[3,4,5] Aleksandr Ramaniuk,[2,5] Van Cao Long,[3] Krzysztof Borzycki,[6] Khoa Dinh Xuan,[1] Mariusz Klimczak,[2,5] and Ryszard Buczyński[2,5]

[1]Department of Physics, Vinh University, 182 Le Duan, Nghe An Province, Vinh City, Vietnam
[2]Faculty of Physics, University of Warsaw, Pasteura 5, 02-093 Warszawa, Poland
[3]Institute of Physics, University of Zielona Góra, Prof. Szafrana 4a, 65-516 Zielona Góra, Poland
[4]Department of Physics, Hong Duc University, 565 Quang Trung, Thanh Hoa City, Vietnam
[5]Department of Glass, Institute of Electronic Materials Technology, Wólczyńska 133, 01-919, Warszawa, Poland
[6]National Institute of Telecommunications, Szachowa 1, 04-894 Warszawa, Poland
*Corresponding author: jpniewski@igf.fuw.edu.pl

Received 3 January 2018; revised 9 March 2018; accepted 21 March 2018; posted 29 March 2018 (Doc. ID 318735); published 3 May 2018

A photonic crystal fiber (PCF) made of fused silica glass, infiltrated with carbon tetrachloride (CCl_4), is proposed as a new source of supercontinuum (SC) light. Guiding properties in terms of effective refractive index, attenuation, and dispersion of the fundamental mode are studied numerically. As a result, two optimized structures are selected and verified against SC generation in detail. The dispersion characteristic of the first structure has the zero-dispersion wavelength at 1.252 μm, while the dispersion characteristic of the second structure is all-normal and equals $-4.37\ \mathrm{ps \cdot nm^{-1} \cdot km^{-1}}$ at 1.55 μm. SC generation was demonstrated for the wavelengths 1.064 μm, 1.35 μm, and 1.55 μm. We prove the possibility of coherent, octave-spanning SC generation with 300 fs pulses with only 0.8 nJ of energy in-coupled into the core with each of the studied structures. Proposed fibers are fully compatible with all-silica fiber systems and PCFs with wide mode area, and can also be used for all-fiber SC sources. The proposed solution may lead to new low-cost all-fiber optical systems.

OCIS codes: (060.5295) Photonic crystal fibers; (320.6629) Supercontinuum generation; (260.2030) Dispersion; (060.4370) Nonlinear optics, fibers.

https://doi.org/10.1364/AO.57.003738

1. INTRODUCTION

Photonic crystal fibers (PCFs) or holey optical fibers have been intensively studied for more than two decades, due to their unique properties compared to bulk media or conventional fibers, that lead to many applications, including fiber light sources [1,2] and sensors [3]. Modifications of the shape, sizes, and positions of air-holes in the microstructured cladding along with the proper choice of a base material allow for the control of dispersion, transmission, and even nonlinear properties of the fibers as well [4,5].

The internal structure of a PCF governs its dispersion characteristic. Several aspects of the exclusive dispersion behavior in PCFs have been already identified, including ultra-flattened dispersion characteristic [6], zero-dispersion wavelength shift [7], and chromatic dispersion optimization [8].

Once a solid PCF is fabricated, it is usually difficult to modulate its optical properties to make it a tunable optical device. Infiltration of PCFs with liquids adds a degree of freedom that enhances the range of possible applications [9,10]. Particularly, the dispersion properties of such fibers can be tuned by a selective hole filling [11,12]. Further modification of guiding properties of the fibers is possible when the temperature is changed, leading to a change of the refractive index of a liquid on the fly [13,14]. For example, in Ref. [14], for a PCF fiber infiltrated with water-ethanol mixture, a 62 nm shift of the zero-dispersion wavelength (ZDW) by changing the temperature or/and the concentration of the water-ethanol mixture was shown.

Owing to the higher nonlinear refractive index of a number of liquids in comparison to fused silica, it is possible to observe

nonlinear phenomena with a lower peak power than in classical solid fibers. For example, the nonlinear refraction index n_2 of carbon tetrachloride (CCl_4) equals 1.53×10^{-19} m^2/W @1.064 μm [15], while in the case of fused silica it is equal to 2.74×10^{-20} m^2/W @1.053 μm [16]. The high nonlinear refractive index is also crucial with respect to the one of the most interesting optical phenomena that is supercontinuum (SC).

A number of works report the possibility of SC generation in liquid-infiltrated PCFs [10,17–25]. In most papers the ultrafast Kerr nonlinearity of such liquids as carbon disulfide (CS_2), toluene, CCl_4, or chloroform ($CHCl_3$) were utilized. Apart from the nonlinear refractive index n_2 higher than fused silica, up to 200 times for CS_2, mentioned liquids are transparent in the visible (VIS) and near-IR (NIR) wavelength range. However, because of high toxicity as well as explosive, carcinogenic, and volatile properties of CS_2, other liquids (ethanol, toluene, $CHCl_3$, or CCl_4) are preferred in real applications.

Different glasses can be used as a base material for PCFs, allowing for efficient SC generation in mid-IR. In Ref. [10] a numerical study of the dispersion characteristic modification of PBG-08 soft glass-based PCFs infiltrated with different liquids was shown. This glass has the light transmission window in the range of 0.4 μm to 5 μm and higher refractive index than fused silica. For a developed fiber, two SC spectra were modeled, for air-hole PCF and toluene-filled PCF, for the pump wavelength 1.55 μm, 100-fs-long pulses and the in-coupled pulse energy 0.5 nJ. The SC spectrum in toluene-filled PCF was redshifted and wider (1.1 μm at 10 dB level) with respect to the air-holes PCF.

The possibility of selective hole infiltration makes further shaping of a PCF's dispersion characteristic viable. Vieweg *et al.* [17] have shown a two-photon direct-laser writing technique that allows for closing of individual air-holes in a PCF and demonstrated SC generation for a PCF infiltrated with CCl_4, when a femtosecond pump was used (210-fs-long pulses at a center wavelength of 1.03 μm). For the beam power of 100 mW a 600-nm-wide SC spectrum was obtained.

A flat dispersion characteristic is crucial for efficient SC generation. A special design of a liquid-filled PCF was presented, where only the first ring of holes surrounding the core was filled with a liquid [18]. It resulted in near-zero ultra-flat dispersion as small as 0 ± 0.41 ps/nm/km for a broad wavelength range of approx. 400 nm, although given within the dynamics of more than 100 dB and with a hypothetical liquid.

A PCF with the central core filled with $CHCl_3$ was also proposed [19]. For a particular design of the PCF's cross-section, a normal dispersion profile in the VIS-to-NIR region was modeled numerically, where the dispersion in the vicinity of 1.06 μm pump wavelength was in the range from −20 ps/nm/km to −50 ps/nm/km. As a result, a flat SC with high degree of coherence spanning near 2 octaves, from 340 nm to 1360 nm at −20 dB level was predicted, when 100 fs pulses are launched in the 0.01-m-long fiber (with 47 kW peak power).

Churin *et al.* modeled numerically and confirmed experimentally the possibility of SC generation in a CS_2-filled 16-cm-long PCF [20]. The PCF was pumped with compact mode-locked fiber lasers pumping at 1.56 μm and 1.91 μm and the SC spanned the wavelength ranges 1.46 μm to 2.1 μm and 1.79 μm to 2.4 μm at 20 dB level.

Recently, a possibility of SC generation in a PCF with the central core filled with toluene was demonstrated. The spectral range of the SC was from 1.0 μm to 1.75 μm, for 450-fs-long pulses, 3 nJ pulse energy, and pump wavelength 1.55 μm [21].

In the paper by Bozolan *et al.* [22] SC generation was demonstrated in a 5-cm-long water-core PCF pumped near water's ZDW. Up to 500-nm-wide spectrum within 20 dB dynamics was achieved, over 4 times more than with a bulk setup, when pumped at 0.98 μm with 100-fs-long pulses. Later, SC generation in the mid-IR wavelength region in 5 μm and 10 μm core diameter capillary fibers filled with CS_2 was also shown [23], allowing for a spectral width of over 1.2 μm and 1 μm, at pump wavelengths of 1.03 μm, 1.51 μm, and 1.685 μm, and with 450-fs-long pulses.

Latterly, a detailed analysis and experimental verification of hybrid soliton dynamics as an important mechanism of SC generation was presented by Chemnitz *et al.* [24], for a capillary fiber filled with CS_2, pumped in the anomalous dispersion regime by a 460 fs laser operating at 1.95 μm. An octave-spanning SC was obtained in the range 1.1 μm to 2.7 μm at 14 nJ pulse energy. It was also shown that existing dispersion does not properly account for the strong absorption of CS_2 at mid-IR wavelengths. Subsequently, soliton-fission mediated infrared SC generation in liquid-core capillary fibers using highly transparent carbon chlorides (CCl_4, C_2Cl_4) were presented [25]. In particular, the C_2Cl_4-core fiber showed octave-spanning bandwidths (1.1 μm to 2.4 μm) with the broadening starting at pulse energies as low as 0.5 nJ, using 270 fs pulses at 1.92 μm wavelength. Generation of vector vortex beams with a liquid core optical fiber was also presented [26].

Further change of the guiding properties of a PCF is possible by the change of the temperature of a liquid or by an external electric field [27,28]. Tunable PCFs can be used, for example, in waveguide sensors [29] or ultrafast couplers [30]. Recently, tunable parametric amplifiers based on PCFs infiltrated with liquids were studied both theoretically [31,32] and experimentally [33].

One of the potential applications of PCFs is optofluidics, a combination of microfluidic devices and optics, and is a promising and rapidly developing technology [34]. In this case PCFs are a good choice leading to practical applications, including waveguides [35] and SC as a light source [36].

In this paper we propose and analyze a PCF made of fused silica glass, infiltrated with CCl_4, for use as a NIR SC source pumped with low-energy pulses. Guiding properties in terms of effective refractive index, attenuation, and dispersion of the fundamental mode are studied numerically. As a result, two setups are analyzed in detail. Next, using generalized nonlinear Schrödinger equation (GNLSE), SC generation is demonstrated for both setups. Finally, the advantages of these fibers are discussed.

We have chosen CCl_4 because its linear refractive index is similar to fused silica, resulting in similar linear properties, and the difference between those two materials can be attributed mainly to the nonlinear refractive index. Hence, it is possible to achieve high coupling efficiency when splicing with fused silica-based fibers having similar core diameters, without the need of using special connectors, something favorable in

all-fiber systems based on fused silica. The nonlinear refraction index of CCl_4 is higher than or comparable to a number of highly nonlinear soft glasses [37]. Although some soft glasses have even higher nonlinear refractive index, splicing then with fused silica is problematic due to huge difference between thermal expansion coefficients [38]. Moreover, transmission losses in soft glasses can be much higher than in the case of liquid-filled PCFs.

2. NUMERICAL MODELING OF THE PCF

The schematic of the geometrical structure of the modeled PCF (cross-section) is shown in Fig. 1, where only three rings of air-holes of the photonic cladding are shown for clarity. The actually modeled PCF consists of eight rings of air-holes ordered in a hexagonal lattice, surrounding the central liquid-filled hole. The linear filling factor of the cladding is defined as $f = d/\Lambda$, where d is the diameter of a single air-hole, and Λ is the lattice constant. We assume that PCF is made of fused silica glass (SCHOTT Lithosil). The central hole is filled with CCl_4. The characteristics of the real and imaginary part of the refractive index of CCl_4 are shown in Fig. 2 [39]. CCl_4 is transparent

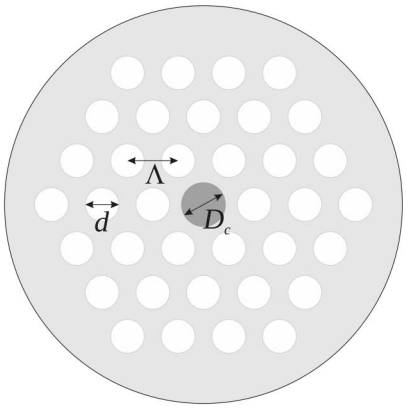

Fig. 1. Schematic of the modeled PCF structure, where D_c is the diameter of the liquid-filled core.

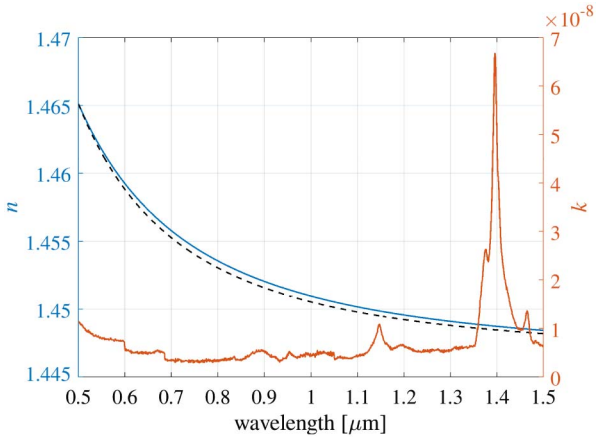

Fig. 2. Characteristics of the real (n) and imaginary (k) part of the refraction index of CCl_4 for the temperature of 20°C [39]. The black-dashed line denotes n of fused silica.

Table 1. Sellmeier's Coefficients for the Materials Used

Coefficient	Value
Fused silica	
B_1	0.6694226
B_2	0.4345839
B_3	0.8716947
C_1	4.4801×10^{-3} μm^2
C_2	1.3285×10^{-2} μm^2
C_3	95.341482 μm^2
Carbon tetrachloride	
B_1	1.09215
C_1	0.01187 μm^2

in a broad range of VIS and NIR wavelengths. The high absorption peak at 1.396 μm reaches k value 6.68×10^{-08}. The attenuation a at this wavelength equals 2.6 dB/m, calculated from the relation below, where λ is the wavelength

$$a = 10 \log[e^{(4\pi k/\lambda)}]. \quad (1)$$

The refractive index of CCl_4 is close to that of fused silica, and the difference between those two materials is attributed mainly to the nonlinear refractive index. The refractive index characteristics are modeled using a Sellmeier's equation as given below, where the C_i coefficients have dimensions of micrometers squared (μm^2),

$$n^2(\lambda) = A_1 + \frac{B_1\lambda^2}{\lambda^2 - C_1} + \frac{B_2\lambda^2}{\lambda^2 - C_2} + \frac{B_3\lambda^2}{\lambda^2 - C_3}. \quad (2)$$

The Sellmeier's coefficients for fused silica and CCl_4 are presented in Table 1.

3. MODELING MODAL AND DISPERSION PROPERTIES OF THE PCF

First, preliminary numerical simulations were conducted for the lattice constants equal to 0.7 μm, 1.0 μm, 1.5 μm, 2.0 μm, 3.0 μm, 4.0 μm, 5.0 μm, and 6.0 μm, and for the filling factors 0.35, 0.4, 0.5, 0.6, and 0.8. As a result, 40 simulation runs were conducted at this stage. For each simulation run the diameter of the core was calculated from the equation $D_c = 2\Lambda - 1.2d$. The smallest core diameter was 0.73 μm for $\Lambda = 0.7$ μm and $f = 0.8$. The biggest core diameter was 9.48 μm for $\Lambda = 6$ μm and $f = 0.35$. A commercial-grade simulator, eigenmode solver, and propagator was used to perform the calculations in the case of modal and dispersion properties of the PCF [40], with the assumption that CCl_4 exhibits negligible losses. This does not influence the dispersion characteristics.

The first ring of air-holes surrounding the core has the main influence on dispersion properties of the fiber, while other rings are responsible for mode attenuation, especially for higher modes. For the modeling we used a constant filling factor for all rings to simplify the future fiber development. At this stage we do not verify if the selected fiber is a single-mode or a multimode fiber. This analysis is performed for optimized fibers.

In Fig. 3 the characteristics of dispersion for the fundamental mode are shown for the wavelength range 0.5 μm to 2 μm.

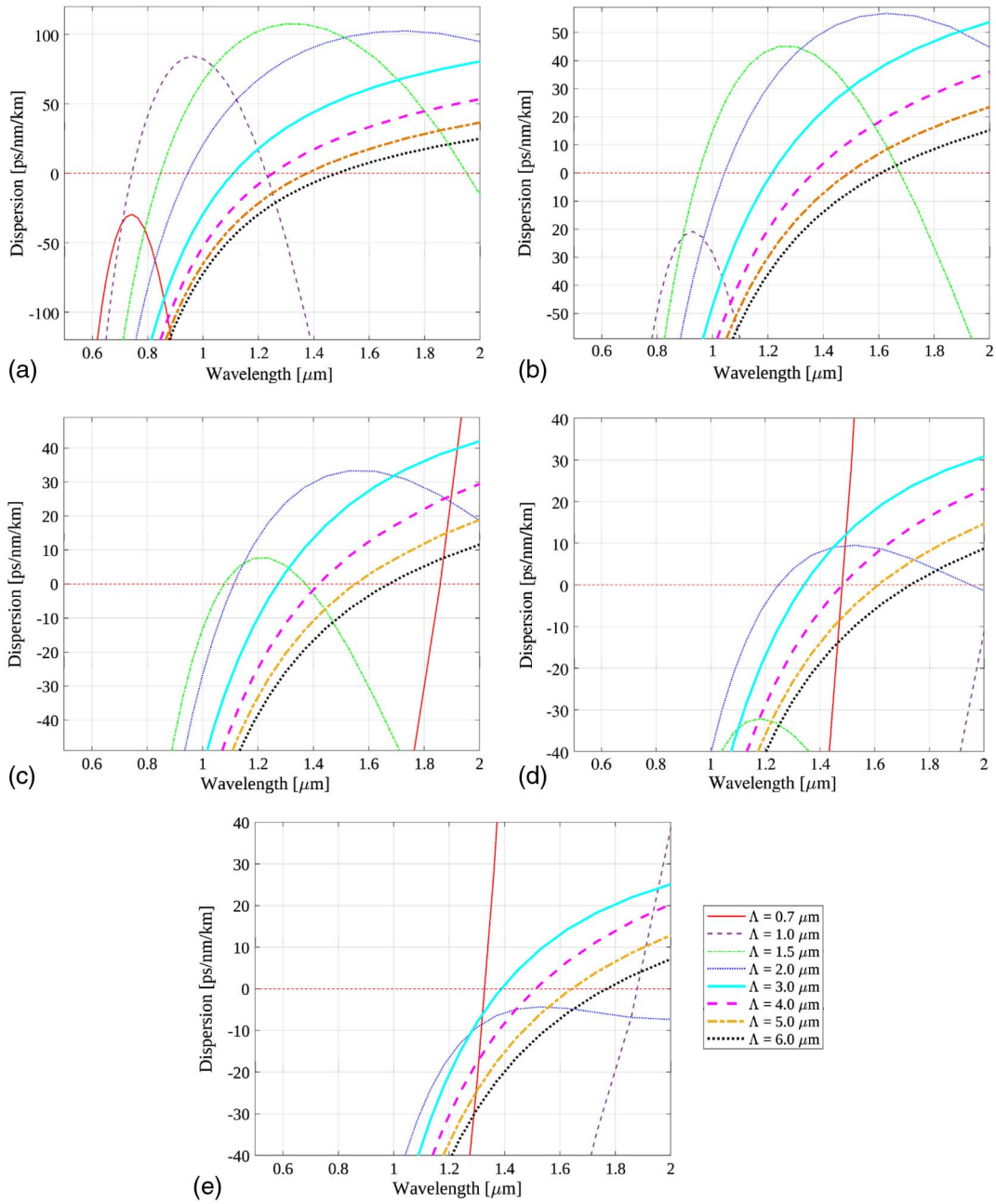

Fig. 3. Characteristics of the fundamental mode dispersion for various filling factor f values equal (a) 0.8, (b) 0.6, (c) 0.5, (d) 0.4, and (e) 0.35. The dotted line denotes zero dispersion. Note: the x-axis limits are set constant for all plots to better show the shift of the characteristics, while the y-axis limits vary.

For a given f value, the characteristics are shifted toward longer waves and flattened with increasing Λ. The same applies to ZDWs. Moreover, for a given Λ, ZDW is usually shifted toward longer waves with decreasing f. For Λ equal to 0.7 μm or 1.0 μm, characteristics are steep and not flat. For high values of Λ the dispersion is lower than 10 $\text{ps} \cdot \text{nm}^{-1} \cdot \text{km}^{-1}$ over the range of 150 nm or more for wavelengths bigger than ZDW.

The optimization criteria aimed at generation of SC at selected wavelengths (1.064 μm, 1.35 μm, 1.55 μm) and followed the analysis in Ref. [41], including the flatness and the sign of the dispersion characteristic, material attenuation, and distance from ZDW if located in the analyzed wavelength range.

On the basis of preliminary calculations we selected two PCFs, namely #F1 ($\Lambda = 4.0$ μm; $f = 0.8$) and #F2 ($\Lambda = 2.0$ μm; $f = 0.35$). These fibers have optimum dispersion characteristics for SC generation, due to the achieved flatness of the anomalous dispersion profile of the #F1 structure as well as to an interesting, all-normal #F2 structure dispersion profile, which is compatible with pumping with either 1.064 μm or 1.55 μm existing femtosecond lasers. The properties of both structures are studied in detail. The material losses

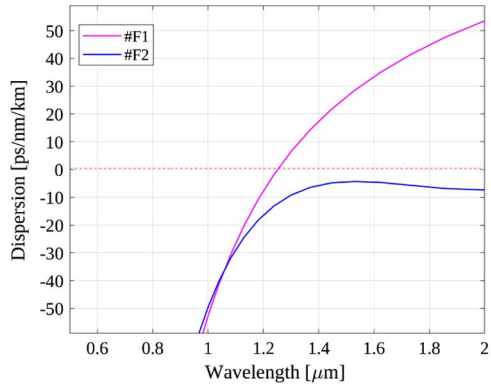

Fig. 4. Characteristics of the fundamental mode dispersion for the fibers #F1 and #F2.

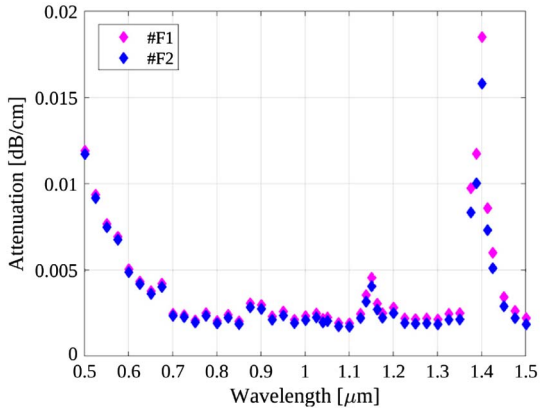

Fig. 5. Characteristics of attenuation of the fundamental mode for the fibers #F1 and #F2.

shown in Fig. 2 were incorporated in calculations. Dispersion characteristics of these two fibers are shown in Fig. 4. Fiber #F1 has ZDW at 1.252 μm and the dispersion at 1.35 μm is equal to 12 $\text{ps} \cdot \text{nm}^{-1} \cdot \text{km}^{-1}$, while #F2 exhibits all-normal dispersion in the whole analyzed wavelength range and the dispersion at 1.55 μm equals $-4.37\ \text{ps} \cdot \text{nm}^{-1} \cdot \text{km}^{-1}$. The dispersion of PCF #F2 is flat at 1.55 μm.

In Fig. 5 attenuation characteristics of the fundamental mode as a function of the wavelength are shown. It is clear that the attenuation characteristics follow the bulk material losses of CCl_4, playing the major role. For the wavelength of 1.4 μm the losses reach the highest values, 0.0185 dB/cm and 0.0158 dB/cm, for #F1 and #F2, respectively. The modal area of the fundamental mode increases almost linearly with the wavelength. For the wavelength of 0.5 μm the modal area equals 9.97 μm^2 for #F1 and 5.946 μm^2 for #F2, while for the wavelength of 1.55 μm the modal area equals 11.83 for #F1 and 10.58 μm^2 for #F2. For #F1 the mode area is higher than for #F2 as a consequence of the bigger structure of the fiber.

4. SIMULATIONS OF SC IN SELECTED FIBERS

To investigate the influence of the infiltration by liquid of the PCF on its nonlinear performance for both discussed fibers #F1 and #F2, we performed numerical simulations of SC generation. The simulations employed numerical solutions of the generalized nonlinear Schrödinger equation (GNLSE), based on the split-step Fourier method.

The following form of GNLSE was used to simulate SC [42],

$$\partial_z \tilde{A} = i\tilde{\beta}(\omega)\tilde{A} - \frac{\tilde{\alpha}(\omega)}{2}\tilde{A} + i\frac{n_2(\omega_0)\omega}{cA_{\text{eff}}(\omega)}\tilde{A}\mathcal{F}\left[\int_{-\infty}^{\infty} R(t')|A|^2(t-t')\mathrm{d}t'\right]. \quad (3)$$

In Eq. (3) we used a time pulse envelope $A(t)$ in the frequency domain, $\tilde{A}(\omega) = \mathcal{F}(A(t))$, where

$$\mathcal{F}[A(t)] = \int_{-\infty}^{\infty} A(t)e^{-i\omega t}\mathrm{d}t \quad (4)$$

denotes the Fourier transform. The linear term consists of a propagation constant in a moving time frame $\tilde{\beta}(\omega) = \beta(\omega) - \beta(\omega_0) - \omega\partial\beta(\omega = \omega_0)$ and an attenuation constant $\tilde{\alpha}(\omega)$ including both material and modal fiber attenuation. The nonlinear coefficient includes the nonlinear refractive index n_2 of CCl_4 and the effective mode area A_{eff}. During the calculations we assumed that all power of the mode is confined inside the liquid core and thus neglected the influence of the electric field inside the cladding. This form of the nonlinear coefficient allows us to use a frequency dependence in a straightforward manner without introducing shock-time corrections. A semiclassical noise is added to the system via one-photon-per-mode noise [42]. The nonlinear response function $R(t')$ is different from functions typically used in SC simulations because of different scattering mechanisms in liquids. Fortunately, in the case of CCl_4 all mechanisms except for the electronic response and the collision-induced polarizability change are negligible, thus nonlinear response function can be written in a simplified manner [43],

$$R(t') = \frac{2n_{el}}{n_2} + n_c\delta(t') + \frac{n_c}{n_2}N_c(1 - e^{-t'/t_r})e^{-t'/t_f}\Theta(t'), \quad (5)$$

where $\delta(t')$ is the Dirac Delta function, $\Theta(t')$ is the Heaviside Theta function, $n_2 = 2n_{el} + n_c$ is the nonlinear refractive index mentioned earlier, and N_c is the normalization constant so that

$$\int_{-\infty}^{\infty} N_c(1 - e^{-t'/t_r})e^{-t'/t_f}\Theta(t') = 1. \quad (6)$$

The first term corresponds to the instantaneous electronic response and depends on the electronic part of the nonlinear coefficient n_{el} only. The second term corresponds to nuclear collisions and depends on the excitation time t_r, the decay time t_f, and the nuclear part of the nonlinear coefficient n_c.

The GNLSE in our model accounts for dispersion terms up to the ninth order and the frequency dependence of the effective mode area. Furthermore, the fiber loss was included in the simulations, although it did not play a significant role after 0.3 m of the assumed fiber's length. The pump pulse adopted in the simulations was Gaussian-shaped and lasted 300 fs (complex amplitude), and the in-coupled energy was ranging from 0.2 nJ to 0.8 nJ. Fractional Raman contribution to nonlinear processes in CCl_4 equals 0.18 [43]. Results of the numerical simulations for the two considered structures are shown in Figs. 6–8, and include numerically generated SC spectra,

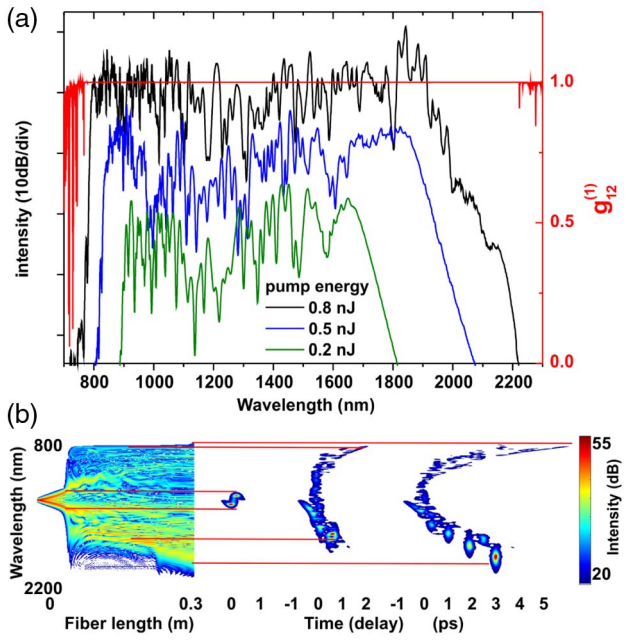

Fig. 6. PCF #F1 pumped with 300 fs, 1.35 μm pulses: (a) spectra of the SC pulses for pump pulse energies of 0.2 nJ, 0.5 nJ, and 0.8 nJ, and degree of coherence calculated from 20 individual pairs of spectra generated with the random noise seed for 0.8 nJ pump pulse; (b) evolution of SC spectrum along the fiber structure, and pulse spectrograms at three different locations along propagation, including from left to right, self-phase modulation, soliton fission, and soliton self-frequency shift accompanied by the dispersive wave generation.

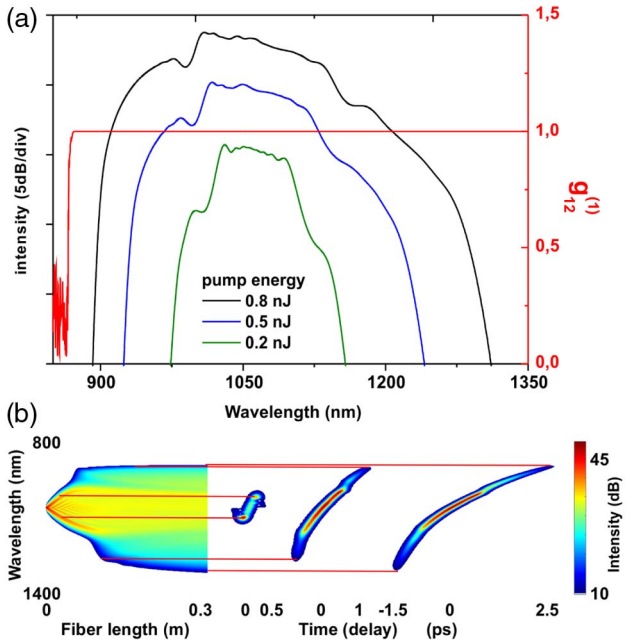

Fig. 7. PCF #F2 pumped with 300 fs, 1.064 μm pulses: (a) spectra of the SC pulses for pump pulse energies of 0.2 nJ, 0.5 nJ, and 0.8 nJ, and degree of coherence calculated from 20 individual pairs of spectra generated with the random noise seed for 0.8 nJ pump pulse; (b) evolution of the SC spectrum along the fiber structure, and pulse spectrograms at three different locations along propagation, including from left to right, self-phase modulation with onset of optical wave breaking, beginning of parametric sideband generation, and completion of spectrum by the optical wave-breaking/parametric sidebands limited by steepening dispersion profile at short wavelengths and by decreasing nonlinearity (increasing mode area) at longer wavelengths. Dispersion-related limitation of the spectral buildup at the blueshifted side is pronounced (compare to 1.55 μm pumped case).

the calculated first-order complex degree of coherence of the generated SC pulses, and the spectral evolution of the pulses along the fibers and in the time domain. Fiber #F1 ZDW of 1.252 μm motivated the use of 1.35 μm pump wavelength for solitonic SC generation, while the all-normal dispersion fiber #F2 was investigated for pumping with standard wavelengths of available femtosecond lasers at around 1.064 μm and 1.55 μm. The wavelength dependence of the coherence degree was calculated from ensembles of the SC spectra (20 individual pairs) according to the formula [41,44]

$$|g_{12}^{(1)}(\lambda, t_1 - t_2 = 0)| = \left| \frac{\langle E_1^*(\lambda, t_1) E_2(\lambda, t_2) \rangle}{[\langle |E_1(\lambda, t_1)|^2 \rangle \langle |E_2(\lambda, t_2)|^2 \rangle]^{1/2}} \right|. \quad (7)$$

Each numerically generated SC pulse in an ensemble had a different random noise seed. The seed was the energy of a single photon with random phase per each simulation bin ("one photon per mode"). Since the femtosecond pump laser was assumed as the initial (pump) pulse source, more sophisticated noise models, like the phase diffusion model [45], have not been used.

Results of the simulations are typical for both normal and anomalous dispersion of PCFs. However, there are significant differences between our CCl_4-filled PCF and both classical silica fiber glasses and other nonlinear liquids. First, CCl_4 nonlinear refractive index n_2 is several times higher than the one measured for fused silica. This allows us to use low-energy pulses. In fact, power of 2.5 kW is sufficient for broad SC generation and is lower than for both fused silica fibers and other previously considered nonlinear liquids. At the same time, attenuation of CCl_4 is smaller than that of nonlinear liquids, such as water, toluene, ethanol, or chloroform [10] and, thus, fiber length can be freely adjusted. Optimal length of the presented PCF is approx. 30 cm, which is more than enough for the development of an octave spanning spectrum under femtosecond pump pulse and would be convenient in handling in a physical experiment. Second, similarity of the refractive index characteristics of fused silica and CCl_4 allows for integration of these two kinds of PCFs. Since the linear refraction index for fused silica is 1.4496 and for CCl_4 is 1.4504 (difference 0.0008) at the wavelength of 1.064 μm, for two PCFs with the same geometry but different cores the numerical aperture would be comparable. Additionally, these fibers are fully compatible with PCFs with wide modal area and can be used for all-fiber SC sources. There is obvious advantage of the high nonlinearity of the fiber structures, above the fact that SC generation develops broadly already for low pump pulse energies. In particular, in the case of #F1 fiber simulations, shown in Fig. 6, it can be seen that the coherence of the SC pulses is maintained up to the largest input pulse energy investigated—0.8 nJ. The evolution of the pulse in the spectral and time domains is otherwise typical, including initial

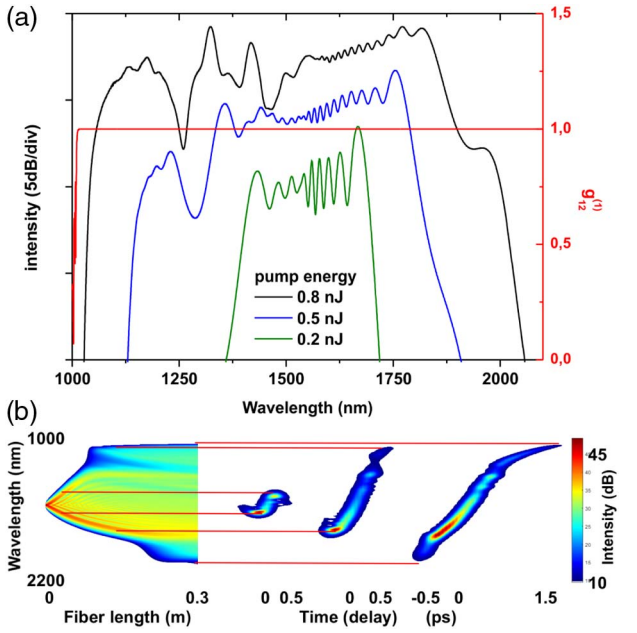

Fig. 8. PCF #F2 pumped with 300 fs, 1.55 μm pulses: (a) spectra of the SC pulses for pump pulse energies of 0.2 nJ, 0.5 nJ, and 0.8 nJ, and degree of coherence calculated from 20 individual pairs of spectra generated with random noise seed for 0.8 nJ pump pulse; (b) evolution of the SC spectrum along the fiber structure, and pulse spectrograms at three different locations along propagation, including from left to right, self-phase modulation with onset of optical wave breaking, beginning of parametric sideband generation, and completion of spectrum by the optical wave-breaking/parametric sidebands limited by steepening dispersion profile at short wavelengths and by decreasing nonlinearity (increasing mode area) at longer wavelengths. Nonlinearity-related limitation of the spectral buildup at the redshifted side is pronounced (compare to 1.064 μm pumped case).

self-phase modulation and extension of the spectrum, accompanied by the compression of the input soliton and its subsequent fission. The spectrum is then completed by a soliton self-frequency shift and accompanying dispersive waves across ZDW—the spectrogram, shown in Fig. 6(b) takes the characteristic "horse-shoe" shape with redshifting solitons and blueshifted dispersive waves. The resulting SC spectrum develops to well over an octave before modulation instability and noise amplification take place; thus, the coherence is maintained. Unfortunately, this still comes at a cost of very complex temporal structure of the pulse, as can be seen in the right-most (output) spectrogram in Fig. 6(b).

Numerically generated spectrograms of the output SC pulse for the case of fiber #F2 pumped with either 1.064 μm or 1.55 μm pulses of 0.8 nJ energy show octave spanning, uniform pulses typical for the self-seeded, femtosecond SC generation at normal dispersion wavelengths. The majority of the energy is contained within a 2 ps to 4 ps time interval. SC pulse pumped at 1.064 μm develops over the shorter wavelengths where there is more normal dispersion, thus the pulse is longer than in the 1.55-μm-pumped case. In each case, the spectrally central part of the pulse is broadened due to self-phase modulation. The temporal elongation as well as almost linear time-wavelength dependence stems from an almost flat chromatic dispersion characteristic, as shown in Fig. 4. Optical wave breaking (OWB) sidebands can be observed at the blueshifted (trailing) edge of the pulse and the redshifted (leading) edge of the pulse. In the 1.55-μm-pumped case (Fig. 8), the redshifted sideband is strongly inhibited due to the decreasing nonlinearity of the fiber, related to increasing of the effective mode area. In-coupling higher pulse energy would have the effect of increased intensity at the trailing edge, although a steep dispersion profile at shorter wavelengths precludes any significant spectral broadening further toward the blue. This can be already observed at around 2.5 ps [Fig. 7(b)] and 1.5 ps [Fig. 8(b)] 1.2 μm area of the output spectrograms, when the trace becomes horizontal over the temporal coordinate (continued elongation in time due to dispersion but no new wavelengths generated by OWB). At the long-wavelength, leading edge, there is still potential for further spectral broadening. However, the limitation here is the increasing mode area, thus decreasing nonlinearity—this can be compensated only by more energetic (or shorter) pump pulses. Owing to the pulse continuity and highly linear time-frequency dependence, the output pulse can be compressed by means of a classical chirp compressor or an all-fiber system [46]. In this specific context it is important to emphasize that recompression down to single optical cycles would require an octave spanning bandwidth and a preserved pulse profile. The advantage of the low pump pulse energy requirement of the fiber #F2, pumped with wavelength of 1.55 μm, can be demonstrated with a simple comparison between the actually discussed structure and a hypothetical fiber structure, where a similar dispersion profile and mode area would be achieved with a standard silica core. This is shown in Fig. 9, for which a simulation shown earlier in Fig. 8 (0.8 nJ of the input energy) is compared to a result obtained for nonlinear refractive index value of CCl_4 substituted with that of silica glass. The resulting SC spectrum with such an assumption hardly has any parametric sidebands developed and is limited to self-phase modulation broadening within roughly 1350 nm to 1750 nm.

The proposed PCF has certain advantages over other types of optical fibers dedicated to SC. Owing to higher nonlinearity of CCl_4 than fused silica, lower power of pulses is required than in case of silica PCFs. At the same time the possibility of dispersion engineering to achieve a flat dispersion characteristic is preserved. The presented CCl_4-filled PCF can also be tuned by means of temperature to modulate the dispersion characteristic and match a given source wavelength. When compared to

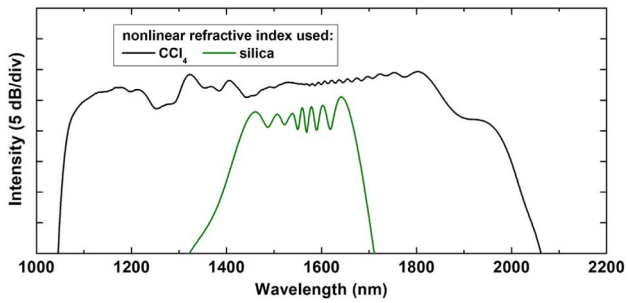

Fig. 9. PCF #F2 pumped at 1.55 μm for the case of CCl_4 filling of the core and for a hypothetical case of silica filling of the core.

soft glass PCFs the proposed fiber has still higher nonlinearity than a number of soft glasses. Moreover, attenuation of soft glass is much higher than in the case of fused silica and bulk CCl_4. This allows for free adjustment of a fiber's length. The advantage of using CCl_4 as a filling medium is that its refractive index is similar to the refractive index of fused silica; thus, it can be easily incorporated in all-fiber optical systems.

5. CONCLUSIONS

A PCF made of fused silica glass, infiltrated with CCl_4, was analyzed numerically. Guiding properties in terms of effective refractive index, attenuation and dispersion of the fundamental mode were studied to obtain flattened VIS-to-NIR SC spectra. Two fiber structures for SC generation were selected and further used for nonlinear modeling using GNLSE. The fiber #F1 has the lattice constant 4.0 μm and the filling factor 0.8. The fiber #F2 has the lattice constant 2.0 μm and the filling factor 0.35. The dispersion characteristic of #F1 has ZDW at 1.252 μm. For #F2 the dispersion characteristic is all-normal and equals $-4.37\ \mathrm{ps}\cdot\mathrm{nm}^{-1}\cdot\mathrm{km}^{-1}$ at 1.55 μm.

SC generation was demonstrated for the wavelengths 1.064 μm, 1.35 μm, and 1.55 μm. Coherent, octave-spanning SC generation was achieved with 300 fs pulses with only 0.8 nJ of energy in-coupled into the core with each of the studied structures. Even less energy, that is 0.5 nJ, was required for a full octave with a solitonic SC generated in the fiber #F1, although at the cost of the expected, complex temporal profile of the output pulse. The all-normal dispersion profile of the fiber #F2 allowed for coherent, full octave spectra to be generated, while maintaining a uniform temporal profile, enabling post-recompression. Importantly, with these structures, standard, fixed-wavelength femtosecond lasers operating at 1.064 μm or 1.55 μm could be used as optical pumps. The low pump pulse requirement, when compared to other types of PCFs, presents an interesting perspective of the CCl_4-filled PCFs in the easing of the output power requirements on the femtosecond mode-locked lasers necessary to obtain octave spanning bandwidths in fiber-based coherent SC.

Funding. Narodowe Centrum Nauki (NCN) (UMO-2016/21/B/ST7/0224); Seventh Framework Programme (FP7) (619205); Fundacja na rzecz Nauki Polskiej (FNP) (TEAM/2016-1/1); Uniwersytet Warszawski (UW) (statutory research).

Acknowledgment. J. Pniewski was supported by the statutory research fund, financed by Faculty of Physics at University of Warsaw.

REFERENCES

1. J. Limpert, T. Schreiber, S. Nolte, H. Zellmer, and A. Tünnermann, "High-power air-clad large-mode-area photonic crystal fiber laser," Opt. Express **11**, 818–823 (2003).
2. J. M. Dudley and G. Genty, "Supercontinuum light," Phys. Today **66** (7), 29–34 (2013).
3. O. Frãzao, J. L. Santos, F. M. Araújo, and L. A. Ferreira, "Optical sensing with photonic crystal fibers," Laser Photon. Rev. **2**, 449–459 (2008).
4. J. C. Knight, "Photonic crystal fibers," Nature **424**, 847–851 (2003).
5. C. M. Smith, N. Venkataraman, M. T. Gallagher, D. Müller, J. A. West, N. F. Borrelli, D. C. Allan, and K. W. Koch, "Low-loss hollow-core silica/air photonic bandgap fiber," Nature **424**, 657–659 (2003).
6. W. H. Reeves, J. C. Knight, P. St.J. Russell, and P. J. Roberts, "Demonstration of ultra-flattened dispersion in photonic crystal fibers," Opt. Express **10**, 609–613 (2002).
7. A. Ferrando, E. Silvestre, P. Andres, J. J. Miret, and M. V. Andres, "Designing the properties of dispersion-flattened photonic crystal fibers," Opt. Express **9**, 687–697 (2001).
8. K. Saitoh, M. Koshiba, T. Hasegawa, and E. Sasaoka, "Chromatic dispersion control in photonic crystal fibers: application to ultra-flattened dispersion," Opt. Express **11**, 843–852 (2003).
9. M. Ebnali-Heidari, F. Dehghan, H. Saghaei, F. Koohi-Kamali, and M. K. Moravvej-Farshi, "Dispersion engineering of photonic crystal fibers by means of fluidic infiltration," J. Mod. Opt. **59**, 1384–1390 (2012).
10. J. Pniewski, T. Stefaniuk, H. Le Van, V. C. Long, L. C. Van, R. Kasztelanic, G. Stępniewski, A. Ramaniuk, M. Trippenbach, and R. Buczyński, "Dispersion engineering in nonlinear soft glass photonic crystal fibers infiltrated with liquids," Appl. Opt. **55**, 5033–5040 (2016).
11. P. S. Maji and P. R. Chaudhuri, "Design of ultra large negative dispersion PCF with selectively tunable liquid infiltration for dispersion compensation," Opt. Commun. **325**, 134–143 (2014).
12. C.-P. Yu and J.-H. Liou, "Selectively liquid-filled photonic crystal fibers for optical devices," Opt. Express **17**, 8729–8734 (2009).
13. P. D. Rasmussen, J. Lægsgaard, and O. Bang, "Chromatic dispersion of liquid-crystal infiltrated capillary tubes and photonic crystal fibers," J. Opt. Soc. Am. B **23**, 2241–2248 (2006).
14. H. L. Van, R. Buczynski, V. C. Long, M. Trippenbach, K. Borzycki, A. N. Manh, and R. Kasztelanic, "Measurement of temperature and concentration influence on the dispersion of fused silica glass photonic crystal fiber infiltrated with water-ethanol mixture," Opt. Commun. **407**, 417–422 (2018).
15. R. L. Sutherland, *Handbook of Nonlinear Optics* (CRC Press, 2003).
16. S. Kedenburg, A. Steinmann, R. Hegenbarth, T. Steinle, and H. Giessen, "Nonlinear refractive indices of nonlinear liquids: wavelength dependence and influence of retarded response," Appl. Phys. B **117**, 803–816 (2014).
17. M. Vieweg, T. Gissibl, S. Pricking, B. T. Kuhlmey, D. C. Wu, B. J. Eggleton, and H. Giessen, "Ultrafast nonlinear optofluidics in selectively liquid-filled photonic crystal fibers," Opt. Express **18**, 25232–25240 (2010).
18. P. S. Maji and P. R. Chaudhuri, "Supercontinuum generation in ultra-flat near zero dispersion PCF with selective liquid infiltration," Optik **125**, 5986–5992 (2014).
19. C. Wang, W. Li, N. Li, and W. Wang, "Numerical simulation of coherent visible-to-near-infrared supercontinuum generation in the $CHCl_3$-filled photonic crystal fiber with 1.06 μm pump pulses," Opt. Laser Technol. **88**, 215–221 (2017).
20. D. Churin, T. N. Nguyen, K. Kieu, R. A. Norwood, and N. Peyghambarian, "Mid-IR supercontinuum generation in an integrated liquid-core optical fiber filled with CS_2," Opt. Mater. Express **3**, 1358–1364 (2013).
21. L. C. Van, A. Anuszkiewicz, A. Ramaniuk, R. Kasztelanic, K. X. Dinh, V. C. Long, M. Trippenbach, and R. Buczynski, "Supercontinuum generation in photonic crystal fibres with core filled with toluene," J. Opt. **19**, 125604 (2017).
22. A. Bozolan, C. J. S. de Matos, C. M. B. Cordeiro, E. M. dos Santos, and J. Travers, "Supercontinuum generation in a water-core photonic crystal fiber," Opt. Express **16**, 9671–9676 (2008).
23. S. Kedenburg, T. Gissibl, T. Steinle, A. Steinmann, and H. Giessen, "Towards integration of a liquid-filled fiber capillary for supercontinuum generation in the 1.2–2.4 μm range," Opt. Express **23**, 8281–8289 (2015).
24. M. Chemnitz, M. Gebhardt, C. Gaida, F. Stutzki, J. Kobelke, J. Limpert, A. Tünnermann, and M. A. Schmidt, "Hybrid soliton dynamics in liquid-core fibres," Nat. Commun. **8**, 42 (2017).
25. M. Chemnitz, C. Gaida, M. Gebhardt, F. Stutzki, J. Kobelke, A. Tünnermann, J. Limpert, and M. A. Schmidt, "Carbon chloride-core fibers for soliton mediated supercontinuum generation," Opt. Express **26**, 3221–3235 (2018).

26. W. Gao, X. Hu, C. Mu, and P. Sun, "Generation of vector vortex beams with a small core multimode liquid core optical fiber," Opt. Express **22**, 11325–11330 (2014).
27. F. Du, Y. Q. Lu, and S. T. Wu, "Electrically tunable liquid-crystal photonic crystal fiber," Appl. Phys. Lett. **85**, 2181–2183 (2004).
28. T. Gissibl, M. Vieweg, M. M. Vogel, M. Aboud Ahmed, T. Graf, and H. Giessen, "Preparation and characterization of a large mode area liquid-filled photonic crystal fiber: transition from isolated to coupled spatial modes," Appl. Phys. B **106**, 521–527 (2012).
29. M. Ebnali-Heidari, F. Koohi-Kamali, A. Ebnali-Heidari, M. K. Moravvej-Farshi, and B. T. Kuhlmey, "Designing tunable microstructure spectroscopic gas sensor using optofluidic hollow-core photonic crystal fiber," IEEE J. Quantum Electron. **50**, 1–8 (2014).
30. M. Vieweg, T. Gissibl, S. Pricking, Y. Kartashov, L. Torner, and H. Giessen, "Tunable ultrafast nonlinear optofluidic coupler," Opt. Lett. **37**, 1058–1060 (2012).
31. P. S. Maji and P. R. Chaudhuri, "Tunable fiber-optic parametric amplifier based on near-zero ultraflat dispersion PCF for communication wavelength," IEEE Photon. J. **7**, 1400313 (2015).
32. S. P. Singh, V. Mishra, P. K. Datta, and S. K. Varshney, "Dispersion engineered capillary-assisted chalcogenide optical fiber based mid-IR parametric sources," J. Lightwave Technol. **33**, 55–61 (2015).
33. L. Velázquez-Ibarra, A. Díez, E. Silvestre, and M. V. Andrés, "Wideband tuning of four-wave mixing in solid-core liquid-filled photonic crystal fibers," Opt. Lett. **41**, 2600–2603 (2016).
34. D. Psaltis, S. R. Quake, and C. Yang, "Developing optofluidic technology through the fusion of microfluidics and optics," Nature **442**, 381–386 (2006).
35. J. Park, D.-E. Kang, B. Paulson, T. Nazari, and K. Oh, "Liquid core photonic crystal fiber with low refractive-index liquids for optofluidic applications," Opt. Express **22**, 17320–17330 (2014).
36. H. Saghaei, M. Ebnali-Heidari, and M. K. Moravvej-Farshi, "Midinfrared supercontinuum generation via As_2Se_3 chalcogenide photonic crystal fibers," Appl. Opt. **54**, 2072–2079 (2015).
37. J. Cimek, N. Liaros, S. Couris, R. Stepien, M. Klimczak, and R. Buczynski, "Experimental investigation of the nonlinear refractive index of various soft glasses dedicated for development of nonlinear photonic crystal fibers," Opt. Mater. Express **7**, 3471–3483 (2017).
38. N. Granzow, S. P. Stark, M. A. Schmidt, A. S. Tverjanovich, L. Wondraczek, and P. St. J. Russell, "Supercontinuum generation in chalcogenide-silica step-index fibers," Opt. Express **19**, 21003–21010 (2011).
39. S. Kedenburg, M. Vieweg, T. Gissibl, and H. Giessen, "Linear refractive index and absorption measurements of nonlinear optical liquids in the visible and near-infrared spectral region," Opt. Mater. Express **2**, 1588–1611 (2012).
40. Lumerical Solutions, Inc., http://www.lumerical.com/tcad-products/mode/.
41. M. Klimczak, B. Siwicki, A. Heidt, and R. Buczyński, "Coherent supercontinuum generation in soft glass photonic crystal fibers," Photon. Res. **5**, 710–727 (2017).
42. J. M. Dudley, G. Genty, and S. Coen, "Supercontinuum generation in photonic crystal fiber," Rev. Mod. Phys. **78**, 1135–1184 (2006).
43. P. Zhao, M. Reichert, T. R. Ensley, W. M. Shensky III, A. G. Mott, D. J. Hagan, and E. W. Van Stryland, "Nonlinear refraction dynamics of solvents and gases," Proc. SPIE **9731**, 97310F (2016).
44. J. M. Dudley and S. Coen, "Coherence properties of supercontinuum spectra generated in photonic crystal and tapered optical fibers," Opt. Lett. **27**, 1180–1182 (2002).
45. M. H. Frosz, "Validation of input-noise model for simulations of supercontinuum generation and rogue waves," Opt. Express **18**, 14778–14787 (2010).
46. H. G. Winful, "Pulse compression in optical fiber filters," Appl. Phys. Lett. **46**, 527–529 (1985).